

UWL REPOSITORY
repository.uwl.ac.uk

The mechanism of chlorogenic acid inhibits lipid oxidation: An investigation using multi-spectroscopic methods and molecular docking

Cao, Qiongju, Huang, Yuan, Zhu, Quan-Fei, Song, Mingwei, Xiong, Shanbai, Manyande, Anne
ORCID: <https://orcid.org/0000-0002-8257-0722> and Du, Hongying (2020) The mechanism of chlorogenic acid inhibits lipid oxidation: An investigation using multi-spectroscopic methods and molecular docking. *Food Chemistry*, 333. p. 127528. ISSN 0308-8146

<http://dx.doi.org/10.1016/j.foodchem.2020.127528>

This is the Accepted Version of the final output.

UWL repository link: <https://repository.uwl.ac.uk/id/eprint/7212/>

Alternative formats: If you require this document in an alternative format, please contact: open.research@uwl.ac.uk

Copyright: Creative Commons: Attribution-Noncommercial-No Derivative Works 4.0

Copyright and moral rights for the publications made accessible in the public portal are retained by the authors and/or other copyright owners and it is a condition of accessing publications that users recognise and abide by the legal requirements associated with these rights.

Take down policy: If you believe that this document breaches copyright, please contact us at open.research@uwl.ac.uk providing details, and we will remove access to the work immediately and investigate your claim.

17 **Abstract:** Endogenous lipase and lipoxygenase play important roles in accelerating lipid oxidation.
18 Polyphenols are a series of commonly used chemicals for preserving fish and seafood products, due to their
19 positive inhibitory effects on lipid oxidation. However, the mechanism involved is still unknown. The
20 inhibitory effects of chlorogenic acid (CGA) on lipase and lipoxygenase were investigated and explored
21 with multi- spectroscopic and molecular docking approaches. Results showed that CGA could inhibit the
22 activities of lipase and lipoxygenase with concentration increased in a highly dose-dependent manner. CGA
23 quenched intrinsic fluorescence intensities of enzymes by static quenching and binding with CGA which
24 led to changes in 3D structures of enzymes. Results of the molecular docking confirmed binding modes,
25 binding sites and major interaction forces between CGA and enzymes, which reduced the corresponding
26 activity. Thus, this study could provide basic mechanisms of the inhibitory effects of polyphenols on lipid
27 oxidation during food preservation.

28

29 **Keywords:** Chlorogenic acid; Lipase; Lipoxygenase; Spectroscopy analysis; Molecular docking;

30 **1 Introduction**

31 Lipase (triacylglycerol acylhydrolases, EC 3.1.1.3) belongs to carboxylesterases and widely exists in
32 animals and plants. It catalyzes the hydrolysis of triglycerides, which contain long-chain fatty acids at sn-2
33 and sn-1 positions, to free fatty acid and glycerol at the lipid-water interface (Cherif & Gargouri, 2009).
34 Hydrolysis products can further be oxidized by lipoxygenase and free radicals. Lipoxygenase (LOX, EC
35 1.13.11.12), a class of protein which contains non-heme iron, specifically catalyzes polyunsaturated fatty
36 acids and fatty acid esters with a 1,4-*cis, cis* pentadiene structure into hydroperoxide (Andreou, et al., 2010).
37 The catalytic site of LOX is composed of metal ion and amino acid residues. LOX oxidizes unsaturated
38 fatty acids and esters into hydro peroxide derivatives (Nikpour, et al., 2013). Previous studies showed that
39 lipase and LOX affect important physiological reactions which are involved in the pathogenesis of various
40 diseases in humans (Schreiber, et al., 2019).

41 Enzymatic reactions are not only closely related to human diseases, but are also associated with lipid
42 oxidation of fish and fish products during transportation, processing and storage. Oxidizing reaction in the
43 muscle tissue leads to undesirable changes and quality deterioration, such as production of off-odor, rancid
44 flavors, and changes in color and texture (Chauhan, et al., 2018). The increasing content of carbonyl
45 compounds and free fatty acid, which are the main products of enzymatic reactions, influence the flavor of
46 meat (Huang & Ahn, 2019). When the concentration of compounds like hexanal, pentanal, 2, 6-nonadienal
47 and 1-octen-3-one, plus 2, 3-octanedione is high enough, it will produce unpleasant odor. Furthermore, when
48 oxidative products of lipid accelerate protein oxidation, some functions for instance, water holding capacity
49 and protein extractability decline with the oxidation proceeding. These lead to the deterioration of protein
50 functional properties during food processing and preservation, for example, loss of moisture, decrease in
51 hardness and emulsion capacity (Utrera, et al., 2015). Therefore, the inhibition of endogenous enzyme-
52 induced lipid oxidation has become more and more important to fish and fish products.

53 Polyphenols, as one of the representative natural antioxidants, have been shown to perform well in
54 inhibiting lipid oxidation during fish processing and preservation. For instance, the combination of tea
55 polyphenols and vacuum packaging treatment used in weever (*Micropterus salmoides*) storage, presented
56 better quality enhancement effects and good quality control which extended the corresponding shelf life at
57 0 °C and 4 °C (Ju, et al., 2018). Glazing treatment with rosemary (*Rosmarinus officinalis*) extract displayed
58 the best performance in controlling protein and lipid changes of mud shrimp (*Solenocera melantho*) stored
59 at -20 °C (Shi, et al., 2019). Furthermore, phenolic compounds such as caffeic acid, coumaric acid, capsaicin,
60 quercetin, epigallocatechingallate (EGCG) showed inhibitory effects on pancreatic lipase *in vitro* (Martinez-
61 Gonzalez, et al., 2017). Chlorogenic acid (CGA), the ester of caffeic acid and quinic acid, is a type of
62 polyphenol widely present in natural plants. CGA exhibits various biological properties which include
63 antioxidant, antibacterial, anti- inflammation (Karar, et al., 2016) and anti-glycation (Gugliucci, et al., 2009).
64 Therefore, the absorption of CGA might induce biological effects in the whole body system, such as
65 protection against cardiovascular disease; and the inhibition of the formation of mutagenic and carcinogenic
66 N-nitroso compounds (Olthof, et al., 2001). Besides the healthy and various biological effects, it has been
67 demonstrated that it is effective in food preservation, for example peach storage (Jiao, et al., 2019) and raw
68 refrigerated chicken (Sun, et al., 2020). In recent years, research on CGA has focused on the preservation
69 of aquatic products. For example, CGA-gelatin combined with partial freezing effectively delayed the decay
70 of sword prawn (*Parapenaeopsis hardwickii*) (Ge, et al., 2020). However, there are very few studies that
71 have demonstrated the application of grass carp preservation in the field. Recently, we found that CGA
72 showed good efficiency in inhibiting lipid oxidation of grass carp muscle during chilled storage (Cao, et al.,
73 2019). However, the mechanism of action of CGA and mode of inhibition of lipid oxidation during fish
74 preservation is still not yet clear. Thus, the interactions between CGA and lipase/lipoxygenase are important

75 for understanding the mechanism of the application of CGA on grass carp preservation.

76 In this study, the interactions of CGA with endogenous enzymes extracted from grass carp muscle were
77 investigated using enzyme activity inhibition assay, intrinsic fluorescence quenching measurement,
78 secondary structure determination and Fourier transform- infrared spectroscopy (FT-IR) measurement.
79 Moreover, the information of binding modes and binding sites of CGA on lipase and LOX were separately
80 explored utilizing the molecular docking method. We aimed to explain or give some insights into the
81 inhibitory mechanism of CGA on lipid oxidation during fish preservation.

82

83 **2 Materials and methods**

84 **2.1 Materials**

85 CGA was purchased from Melonepharma (Dalian, Liaoning, China) while 4-nitrophenyl butyrate (4-
86 NPB) was obtained from Sigma–Aldrich Chemical Co (St. Louis, MO, USA) and linoleic acid from Aladdin
87 (Shanghai, China). Protein loading buffer (5×) was purchased from Kerui (Wuhan, Hubei, China). All
88 reagents and chemicals used were of analytical grade.

89 **2.2 Fish sample preparation**

90 All procedures were approved by the Animal Care and Use Committee of Huazhong Agricultural
91 University and performed in accordance with the Guidelines for Care and Use of Laboratory Animals of
92 Huazhong Agricultural University. Fresh grass carp (3.5 ± 0.5 kg, $n=10$) were purchased from a local fish
93 market (Wuhan, Hubei, China). The sampled fish were anaesthetized using MS - 222 (100 mg/L, 3-
94 Aminobenzoic acid ethyl ester methanesulfonate, Shanghai yuanye Bio-Technology Co., Ltd, Shanghai, P.R.
95 China) and were unconscious before slaughter. Then the fish were immediately decapitated and gutted, and
96 the red muscle under the skin was removed, and the white muscle collected, weighed and mixed for further
97 study.

98 **2.3 Extraction of endogenous enzymes**

99 The extraction of lipase was carried out following the Smichi method (Smichi, et al., 2013). The fish
100 muscle sample was homogenized in ten times volume (1:10, *w/v*) 25mM Tris-HCl buffer (pH=8.0, 4 °C,
101 150 mM NaCl, 2 mM benzamidine) with a blender (Y-QSJ1, Oidire, German) for 3×10 s (4000 rpm). Then
102 the mixture was stirred with a magnetic bar (Thermo, Massachusetts, USA) for 45 min (4 °C), and
103 centrifuged for 20min (4 °C, 10000×g). The supernatant was collected and ammonium sulphate added (40%
104 of the supernatant weight). The mixture was stirred for 45 min at 4 °C, and centrifuged at 10000×g for 15
105 min. The supernatant was collected and ammonium sulphate added to 60% saturation. Lastly, the solution
106 was stirred and centrifuged using the same procedure, and the sediment (lipase) was collected into a dialysis
107 bag for desalting with former Tris-HCl buffer for 24h, and the buffer was changed every 6h.

108 The lipoxygenase (LOX) was extracted according to a former method (Gata, et al., 1996). Generally,
109 the fish muscle sample was homogenized in five times volume (*v/m*: 5:1) phosphate buffer (pH=7.4, 50mM,
110 1mM Dithiothreitol, 1 mM Ethylenediaminetetraacetic acid (EDTA)) with a blender (4000 rpm, 4×10s).
111 The mixture was stirred with a magnetic bar at 4 °C for 30min, and further centrifuged (4 °C, 10000×g) for
112 20min. The supernatant was collected and filtrated through a gauze to obtain a crude enzyme solution. To
113 the crude solution was added ammonium sulphate to 20% saturation, stirred for 45min (4 °C) and then
114 centrifuged for 15 min (4 °C, 10000×g). The supernatant was collected and ammonium sulphate added to
115 40% saturation, stirred and centrifuged with former parameters. Finally, the sediment (LOX) was collected
116 and dialyzed following the same extraction procedure of lipase.

117 **2.4 SDS-PAGE (Sodium dodecyl sulfate - polyacrylamide gel electrophoresis)**

118 The protein content in a sample was determined with the Lowry method (Lowry, et al., 1951), and the
119 molecular weight of the endogenous enzyme was determined using SDS-PAGE analysis (n=4). The detailed

120 procedure of the SDS-PAGE was describe in our previous study (Huo, et al., 2016) with slight modification
121 of the solution. The best concentration of separating gel was set to 10%. After electrophoresis, the gel was
122 stained with ~0.1% (w/v, 0.29g in 250 ml) Coomassie blue R-250, dissolved with the solution (250 ml) of
123 8% (v/v) acetic acid and 25% (v/v) ethanol (95%); and destained overnight in 8% (v/v) acetic acid and 25%
124 (v/v) ethanol (95%). The markers of proteins (10 to 250 kDa) were also run in parallel on the same gel to
125 determine the molecular weights of the protein.

126 **2.5 Enzyme inhibition assay**

127 Lipase activity was determined using the 4-NPB method (n=3) (Kuepethkaew, et al., 2017). The
128 substrate solution was prepared by dissolving 4-NPB in isopropanol. The reaction was carried out by mixing
129 800 μ L diluted lipase, 800 μ L CGA solution, and 2.0 mL 50 mM Tris-HCl buffer (pH=8.0, containing 0.5 %
130 Tritox X 100, 25mM NaCl). The reaction was initialized with the addition of 400 μ L substrate solution, and
131 the mixture reacted at 37 $^{\circ}$ C for 15 min. The absorbance was measured with ultraviolet-visible
132 spectrophotometer at 410 nm and one unit of enzyme activity was defined as the enzyme liberated per μ mol
133 of p-nitrophenol in 1 minute. There were three types of inhibition experiments performed with different
134 concentrations of solution. For the inhibition ratio, the concentrations of lipase and 4-NPB solution were
135 0.1mg/mL and 3mM, respectively. For the inhibition type experiments, the following concentrations were
136 used: lipase: 0.025, 0.05, 0.1, 0.2, 0.3 mg/mL; CGA: 0, 0.1, 0.2, 0.3 mg/mL; 4-NPB: 3mM. For the inhibition
137 kinetics experiments, the following concentrations were investigated: lipid: 0.1mg/mL; CGA: 0, 0.1, 0.2,
138 0.3 mg/mL; 4-NPB: 1, 2, 3, 4, 5 mmol/L.

139 LOX's activity was measured according to a former method (n=3) (Gata, et al., 1996). The substrate
140 solution of LOX was prepared by dissolving linoleic acid in distilled water (10 mL, 180 μ L Tween 20) and
141 the pH value was adjusted to 9.0 with 2 M NaOH. Subsequently, 200 μ L diluted LOX solution was mixed

142 with 200 μ L CGA solution and 50 mM citric acid buffer (pH=5.5, 2.4mL), and the mixed solution was
143 incubated for 10 min (25 $^{\circ}$ C). Then, 200 μ L substrate solution was added to initialize the reaction. One
144 minute after the reaction, the absorbance at 234 nm was recorded. One unit of LOX's activity was defined
145 as an increase of absorbance at 234 nm of 0.001 per min under assay condition (Gata, et al., 1996). For the
146 inhibition ratio, the concentrations of LOX and linoleic acid were 0.1 mg/mL and 20 mM, respectively. For
147 the inhibition type experiments, the following concentrations were used: LOX: 0.05, 0.1, 0.2, 0.3, 0.4
148 mg/mL; CGA: 0, 0.05, 0.1, 0.2 mg/mL; linoleic acid: 15 mM. For the inhibition kinetics experiments, the
149 following concentrations were investigated: LOX: 0.1 mg/mL; CGA: 0, 0.05, 0.1, 0.2 mg/mL; linoleic acid:
150 5, 10, 15, 20, 25 mmol/L.

151 **2.6 Fluorescence spectra measurements**

152 The detected enzyme solution (0.1mg/mL) contains relative buffer and different concentrations
153 of CGA (0 M to 40.0 $\times 10^{-6}$ M, stepped by 5 $\times 10^{-6}$ M). The fluorescence spectra of the sample (n=3
154 for every group) were recorded on F-4500 fluorescence spectrometer (Hitachi, Japan) after standing
155 for 30 min to equilibrate, and the fluorescence measurement was performed at three different
156 temperatures (298K, 303K and 310K). The fluorescence intensity was corrected using the following
157 equation:

$$158 \quad F_{corr} = F_{obs} \times e^{(A_{ex}+A_{em})/2} \quad (1)$$

159 where F_{cor} and F_{obs} refer to the corrected and observed fluorescence intensities, respectively. A_{ex} and A_{em}
160 represented the absorption of the ligand at excitation and emission wavelengths, respectively.

161 For the fluorescence quenching measurement, the following parameters were set: excitation wavelength:
162 280 nm; emission slits: 5 nm; voltage: 400V; scanning rate: 1200 nm/min; and emission spectra: 290 to 450
163 nm. For synchronous fluorescence spectra, several parameters were changed: the intervals between emission

164 and excitation wavelength ($\Delta\lambda$): 15 nm and 60 nm; emission spectra: 240 to 310 nm.

165 **2.7 Ultraviolet-visible (UV-VIS) absorption spectra measurements**

166 The detected enzyme solution (0.1 mg/mL) containing relative buffer and different concentrations of
167 CGA (0 to 40×10^{-6} M, stepped by 10×10^{-6} M) were detected with UV-2600 spectrophotometer (UNIC,
168 China) and performed in the range of 230 - 450 nm at room temperature (n=3 for every group) .

169 **2.8 Circular dichroism (CD) spectra measurements**

170 The changes in secondary structures of endogenous enzymes before and after adding CGA were
171 recorded by a Jasco-1500 spectrophotometer (JASCO, Japan) 2.0 mm path length cell at room temperature
172 (n=3 for every group). The constant concentration of enzymes was 0.05mg/mL, CGA concentrations in the
173 complexes were 0, 20.0 and 40.0×10^{-6} M. The CD spectra were recorded from 190 to 250 nm with a scan
174 rate of 200 nm /min, the response time was 2 s. The spectra data were converted to mean ellipticity in deg
175 $\text{cm}^2 \text{dmol}^{-1}$ to calculate the secondary structure of enzymes.

176 **2.9 Fourier transform infrared (FT-IR) spectroscopy measurements**

177 The FT-IR spectra were recorded by a Nicolet470 FT-IR spectrometer (Nicolet, USA) (n=3 for every
178 group). The detected enzyme solutions (0.1 mg/mL) containing various CGA (0.0, 20.0 and 40.0×10^{-6}
179 mol/L) were lyophilized for measurement, and the KBr disc was prepared and measured by adding KBr
180 with or without samples. The spectra were scanned in the range of 500-4000 cm^{-1} with 64 scans and 4 cm^{-1}
181 resolutions. Background spectrum was recorded before each sample measurement.

182 **2.10 Dynamic light scattering (DLS)**

183 The enzyme solution (0.01 mg/mL) containing relative buffer and different concentrations of CGA (0
184 to 4×10^{-6} M, stepped by 1×10^{-6} M) was detected by light scattering determined with Zetasizer Nano ZS90
185 (Malvern, UK). Each measurement was performed with 11 scans and each sample (n=3 for every group)

186 replicated three times.

187 **2.11 Molecular docking**

188 The interaction between CGA and lipase or LOX were simulated using the molecular docking method
189 performed with CDOCKER module available in Discovery Studio 2016 (BIOVIA, USA). The structures of
190 CGA were collected from PubChem (<http://pubchem.ncbi.nlm.nih.gov/>), and the crystal structures of lipase
191 (Protein Data Bank (PDB) ID: 1ETH) and LOX (PDB ID: 2P0M) were downloaded from PDB
192 (<http://www.rcsb.org/>).

193 To prepare protein structures, several steps were initially completed in the software, such as the removal
194 of water molecules and addition of hydrogen atoms. The structure of CGA was optimized due to minimized
195 energy. The docking between CGA and proteins was based on CHARMM force field. The top hit value was
196 set to 10, pose cluster radius was set to 0.5, other docking parameters were default if not mentioned. The
197 lipase-CGA and LOX-CGA interactions are illustrated in 3D and 2D diagrams using Discovery Studio (Xu,
198 et al., 2019).

199 **2.12 Statistical analysis**

200 Statistical analysis was performed with SPSS 22.0 (IBM, New York, USA) using one-way ANOVA.
201 Duncan(D) adjustment was used to determine the significant difference between different groups.
202 Significant differences were declared at $p < 0.05$. The results were expressed as means \pm SD (standard
203 deviation).

204

205 **3 Results and discussion**

206 **3.1 SDS-PAGE analysis of endogenous enzymes in fish flesh**

207 The purity of enzymes was confirmed by SDS-PAGE, and the results are shown in Fig. 1a. The
208 molecular weights of lipase and LOX were about 36 kDa and 97 kDa, and the results are illustrated in Fig.
209 1a-sample 5 and 1a-sample 3. The molecular weight of LOX is similar to that reported in mackerel (*Scomber*

210 *scombrus*) and ham (Banerjee, 2006), and the molecular weight of lipase was also found in grey mullet and
211 whiteleg shrimp (Smichi, et al., 2013).

212 **3.2 Inhibitory activities and inhibition kinetics for endogenous enzymes**

213 The inhibitory activities of endogenous lipase and LOX in fish flesh were investigated and the results
214 are illustrated in Fig. 1b-1d. For the inhibitory ratio, the inhibition curves under different concentrations of
215 CGA on the activities of endogenous enzymes were constructed (Fig.1b1 and 1b2). Results show that
216 inhibitory ratios of CGA against enzyme activities were increased with the addition of CGA. The IC₅₀ values
217 of CGA on lipase and LOX were 0.58 and 0.32 mg/mL, respectively. Results indicate that CGA was an
218 efficient inhibitor for both lipase and LOX and had significantly stronger inhibitory activity for LOX
219 compared with lipase. The kinetic plots of CGA inhibiting lipase and LOX under the same conditions were
220 explored to elucidate the effects (Fig. 1c). As shown in Fig. 1c1 and 1c2, a group of straight lines passed
221 through the origin point, thus both the inhibition processes of CGA on lipase and LOX were reversible (Yu,
222 et al., 2019).

223 For the inhibitory kinetics study, the double reciprocal plot or Lineweaver-Burk plot was employed to
224 analyze the kinetics parameters, Michaelis-Menten constant (K_m) and the maximum velocity (V_m), in the
225 presence of CGA and 4-npb/ linoleic acid (Fig.1d1 and 1d2). For lipase, the addition of CGA increased the
226 K_m value (from 0.93 mg/mL to 2.06 mg/mL), but the V_m (0.01/min) was constant, which indicates that CGA
227 competitively inhibited lipase activity due to binding to the catalytic site of enzymes. The free enzyme
228 inhibition constant (K_i) was 0.23 mg/mL for the lipase inhibition measurement. The competitive inhibition
229 of pancreatic lipase was also reported for compounds extracted from plants such as Ligupurpuroside B and
230 tea saponin (Ying, et al., 2018). For LOX, the increasing value of K_m (from 4.16 mg/mL to 5.03 mg/mL)
231 and decreasing value of V_m (from 0.22/min to 0.16/min) indicates that there is mixed type inhibition. Results

232 imply that CGA might bind to LOX and linoleic acid-LOX complex simultaneously (Yu, et al., 2019).
233 Similar results were also reported in the inhibition of mackerel (*Scomber scombrus*) muscle lipoxygenase
234 by green tea polyphenols (Sreeparna, 2006). Finally, the K_i and the bound enzyme inhibition constant (K_{is})
235 were found to be 0.32 mg/mL and 0.57 mg/mL.

236 3.3 Fluorescence quenching

237 The effect of CGA on tertiary structures of enzymes could be evaluated by the intrinsic fluorescence,
238 which indicates the interactions of CGA and amino acids in aromatic ring structures in proteins including
239 tryptophan (Trp), tyrosine (Tyr) and phenylalanine (Phe) (Cysewski, 2008). The fluorescence emission
240 spectra of lipase and LOX in the presence of different concentrations of CGA at 298K were studied (Fig.
241 2a1 and 2a2). The fluorescence intensities of enzymes were decreased following an increase in CGA and
242 were decreased 44.35% and 60.20% for lipase and LOX respectively. The quenching effects of intrinsic
243 fluorescence indicate the existence of interactions between enzymes and CGA. The intrinsic fluorescence
244 of LOX is easily quenched with CGA, which means there are more opportunities for interaction between
245 CGA and LOX. The results could explain the stronger inhibition of LOX with CGA than with lipase. As
246 shown in Fig. 2a2, the slight redshift in maximum emission wavelength of LOX suggest the increasing
247 hydrophilic microenvironment around fluorophore and amino acid residues after binding with CGA (Xiong,
248 et al., 2016). Furthermore, similar variation tendency was obtained for the fluorescence spectra of lipase
249 and LOX in the presence of different concentrations of CGA at 304K and 310K (Data not shown).

250 3.3.1 Mechanism of fluorescence quenching

251 The quenching mechanism by small molecule quenchers can be classified as static quenching and
252 dynamic quenching, which can be analyzed using the Stern-Volmer equation (Lakowicz, Joseph, 2006):

$$253 \quad \frac{F_0}{F} = 1 + K_{SV}[Q] = 1 + K_q\tau_0[Q] \quad (2)$$

254 where F_0 and F are the fluorescence intensities of the complex without and with CGA, respectively; K_{sv} is
255 the quenching constant; K_q is the quenching rate constant of the biomolecule; $[Q]$ is the concentration of
256 CGA and τ_0 is the average life time of molecules in the absence of the quencher (the value is
257 approximately 10^{-8} s^{-1}).

258 As shown in Fig. 2b1 and Fig. 2b2, the Stern-Volmer curves show good liner relationships. The K_{sv} and
259 K_q for the interactions between CGA and enzymes at different temperatures were collected in Table 1. The
260 K_q of lipase and LOX were $2.11 \times 10^{12} \text{ L/mol}\cdot\text{s}$ and $3.94 \times 10^{12} \text{ L/mol}\cdot\text{s}$ at 298K respectively, which were
261 much higher than the maximum dispersion collision quenching constant ($2.00 \times 10^{10} \text{ L/mol}\cdot\text{s}$). The results
262 suggest that the formation of complexes between CGA and endogenous enzymes and the quenching types
263 of lipase and LOX caused by CGA belong to static quenching. Besides, the K_{sv} values of both interaction
264 systems decreased with increasing temperature, which also presented the characteristics of fluorescence
265 static quenching.

266 The binding constant (K_a) and the number of binding sites (n) of the static quenching process were
267 further evaluated by the following equation (Lakowicz, Joseph R, 2000):

$$268 \quad \log \frac{F_0 - F}{F} = \log K_a + n \log [Q] \quad (3)$$

269 where F_0 and F are fluorescence intensities of the complex without and with CGA, $[Q]$ is the concentration
270 of CGA. As listed in Table 1, the K_a values of lipase-CGA complexes were lower than those of LOX-CGA
271 complexes at different temperatures. The decreased trend of K_a values of the temperature also show that the
272 CGA which induced the quenching mechanism of two types of enzymes was static quenching. The values
273 of n were approximately equal to 1, which demonstrate that there was only one class of binding site for
274 CGA on two types of enzymes and the formation of complexes in intermolecular interactions at a molar
275 ratio of 1:1. The values of K_a and n decreased with increasing temperature, which might have been caused

276 by the decomposition of enzyme-CGA complex.

277 3.3.2 Thermodynamic parameters

278 The Van't Hoff equation (Function 4) and Gibbs equation (Function 5) were used to calculate the
279 thermodynamic parameters of interactions between small molecules and proteins (Ross & Subramanian,
280 1981):

$$281 \ln K_a = -\frac{\Delta H}{RT} + \frac{\Delta S}{R} \quad (4)$$

$$282 \Delta G = \Delta H - T\Delta S \quad (5)$$

283 where K_a is the binding constant at different temperature T (298K, 304K, 310K); ΔH , ΔS and ΔG are the
284 changes of enthalpy, entropy and free energy, respectively; R is the gas constant (8.314 J/mol·K).

285 The values of ΔH , ΔS and ΔG are presented in Table 1, the negative values of ΔH and ΔS show that
286 the hydrogen bond and Van der Waals force interactions might play a major role during the binding process
287 of both lipase-CGA and LOX-CGA systems (Ross & Subramanian, 1981). The negative values of ΔG
288 suggest that the interactions between endogenous enzymes of fish flesh and CGA were spontaneous.

289 3.4 Synchronous fluorescence spectra analysis

290 The synchronous fluorescence spectroscopy is often used to analyze microenvironment changes
291 surrounding amino acid fluorophore residues and study protein conformation changes. The $\Delta\lambda$ between
292 emission wavelength and excitation wavelength established at 15 nm and 60 nm reflect the spectra features
293 of Tyr and Trp, respectively.

294 As shown in Figs. 2c1, c2 and Figs. 2d1, d2, the synchronous fluorescence intensities of Tyr and Trp
295 were both decreased following an increase in CGA. For $\Delta\lambda=15$ nm, a weak blue shift trend of maximum
296 emission wavelength was observed with the gradual addition of CGA into the lipase solution (Fig. 2c1), but
297 there was no shift observed for LOX (Fig. 2c2), which indicates that the interaction between lipase and

298 CGA slightly increased the hydrophobicity of microenvironment around Tyr residues (Peng, et al., 2016).
299 For $\Delta\lambda=60$ nm, there was no obvious shift found in lipase (Fig. 2d1), a small red shift of maximum emission
300 wavelength in LOX (Fig. 2d2) suggests that the addition of CGA slightly improved the polarity of the Trp
301 residue microenvironment (Zhu, et al., 2017). The results imply that CGA may be closer to the Trp residue
302 than Try residue in the LOX-CGA interaction, but it might not bind closer to neither Tyr nor Trp in lipase.
303 According to the above results, there was no significant change in the enzymatic amino acid
304 microenvironment. The changes in maximum emission wavelength with synchronous fluorescence are
305 basically consistent with the results of former fluorescence quenching analysis.

306 **3.5 UV-VIS spectroscopy analysis**

307 UV-VIS absorption spectroscopy is a simple and useful method for investigating protein structural
308 changes. The interactions of lipase/LOX, and CGA at different concentrations were studied using UV-VIS
309 spectroscopy. As shown in Fig. 3a1 and Fig. 3a2, with the continuous increase in CGA concentration, the
310 absorption peaks around 220 nm were gradually increased with a small blue shift indicating that CGA
311 influenced the skeleton structures of these two types of endogenous enzymes (Farhadian, et al., 2019). The
312 increased absorption intensity and red shift of peaks around 275 nm suggest the formation of complexes
313 between enzymes and CGA. The absorbance of lipase-CGA and LOX-CGA complexes was significantly
314 elevated with increasing concentrations between 250 nm and 350 nm. This implies that CGA could lead to
315 the modification of polarity and hydrophilicity of microenvironment around aromatic amino acid residues
316 of endogenous enzymes, which are responsible for changes of lipase and LOX conformation (Menezes, et
317 al., 2019). Moreover, the shift of maximum emission wavelength and differences in UV spectra reconfirmed
318 the fluorescence quenching of interactions between lipase/LOX and CGA was static quenching instead of
319 dynamic quenching, which is similar former results presented in fluorescence quenching spectra (Zhu, et

320 al., 2017).

321 **3.6 CD spectra analysis**

322 The CD spectroscopy has been widely used to determine the changes in protein conformation. Different
323 secondary structures of protein have different characteristic absorption bands in CD spectra. The fractions
324 of α -helix, β -sheet, β -turn and random coil in lipase and LOX without or with CGA are presented in Table
325 2. Following an increase in CGA concentration, lipase's α -helix content decreased, while the contents of β -
326 sheet and β -turn increased, and there was no apparent change observed in random coil content. Results
327 support the notion that the binding of CGA and lipase might destroy the hydrogen and van der Waals' bonds
328 in the secondary structure of lipase, which could lead to the extension of the spiral structure (Zhu, et al.,
329 2018). The α -helix around the catalytic site of lipase stabilizes the enzyme, thus the loss of helical content
330 might result in the destabilization of the structure of spatial protein (Su, et al., 2016).

331 On the other hand, the fractions of α -helix and β -sheet in the secondary structure of LOX increased,
332 instead of decreasing in β -turn and random coil, which suggests that the secondary structure of LOX might
333 be more firming after binding with CGA. The electrostatic interactions might have led to the increase in α -
334 helix content (Shen, et al., 2019). The results described above indicate that the interactions with CGA
335 affected the secondary structure of enzymes, and may have further hampered enzymatic catalytic sites and
336 active centers, affecting the activity of enzymes (Peng, et al., 2016). The results are in accordance with the
337 conclusion obtained from inhibitory effects of CGA on enzymatic activities in this study.

338 **3.7 FT-IR spectra studies**

339 The conformational changes of enzymes affected by CGA could also be investigated through FT-IR
340 spectra. As shown in Fig. 3b1 and Fig. 3b2, the FT-IR spectra of free enzymes and enzyme-CGA complexes
341 in the region of 4000-400 cm^{-1} were investigated. In spectroscopy of lipase-CGA complex (Fig. 3b1), the

342 peak (3229 cm^{-1}) might be associated with the N-H stretching vibration and the peak (2989 cm^{-1}) with
343 asymmetrical stretch of C-H (He, et al., 2018). The amide I ($1700\text{-}1600\text{ cm}^{-1}$) peak with the wavenumber at
344 1632 cm^{-1} originated from C=O stretching vibration. The amide II ($1600\text{-}1500\text{ cm}^{-1}$) peaks which appeared
345 around 1550 cm^{-1} resulted from C-N stretching and N-H bending vibrations (Zhu, et al., 2019). The
346 intensities of these peaks increased compared to those in free lipase.

347 In spectroscopy of the LOX-CGA complex (Fig. 3b2), there was a slight deviation and shift of the
348 amide A peak at 3446 cm^{-1} , which originated mainly from the O-H stretching vibration and the N-H
349 stretching vibration, compared to LOX. The broader band at 2450 cm^{-1} and the shift at 1138 cm^{-1} might be
350 associated with intermolecular interactions. The intensities of peaks were slightly changed during the
351 interaction. The results confirm that interactions exist between CGA and enzymes, and hydrogen bonds are
352 the important force in complexes. The changes of spectra in amide I and amide II infrared absorption bands
353 suggest that CGA not only interacted with lipase and LOX, but also altered the secondary structures of
354 enzymes, which is consistent with results of CD spectra analysis.

355 **3.8 Particle size analysis**

356 The average particle sizes of enzyme-CGA complexes were investigated. Following the elevation of
357 CGA concentration, the average diameters of lipase increased from $1083\pm 14\text{ nm}$ to $1314\pm 18\text{ nm}$ (Fig. 3c1),
358 which confirm that the formation of lipase-CGA complex and CGA could cause the aggregation of lipase.
359 However, the average particle size of LOX only slightly increased from $149\pm 1\text{ nm}$ to $155\pm 1\text{ nm}$ (Fig.
360 3c2), which suggests that the complex might be formed between LOX and CGA, but the aggregation of the
361 enzyme was not obvious. The difference might be attributed to the different structures of lipase and LOX.
362 These phenomena are similar to those reported between wine polyphenols and yeast protein extract,
363 mannoproteins (Neguela, et al., 2016). The particle size distribution of enzyme-CGA complexes in Fig. 3d1

364 and Fig.3 d2 illustrates that lipase has a wider particle size distribution than LOX following the increase in
365 CGA concentration, which is consistent with former results (Zhu, et al., 2017).

366 **3.9 Molecular docking analysis**

367 Molecular docking is an effective and reliable computational technique for predicting possible binding
368 modes and studying ligand binding mechanisms of small molecules and protein. In this study, for the sake
369 of exploring deeper insight into the nature of the interactions between lipase/LOX and CGA theoretically,
370 the molecular docking method was used to analyze the binding process based on the CDOCKER protocol.

371 The docking interaction plots at the best active sites of enzymes are illustrated in Fig. 4a and Fig. 4b,
372 and the interaction details between the amino acid residues and CGA in different conditions from 3D
373 docking mode and 2D schematic diagram are demonstrated in Fig. 4c-d. It can clearly be seen that CGA
374 formed hydrogen bonds with lipase (Fig. 4c1), including conventional hydrogen bond with aspartic (Asp)
375 80 (Bond length-2.33 Å), carbon hydrogen bonds with catalytic residue serine (Ser) 153 (3.07 Å) and
376 arginine (Arg) 257 (2.86 Å), π -donor hydrogen bond with histidine (His) 264 (3.16 Å). Besides, hydrophobic
377 interactions between the benzene ring and Trp 253 (5.32 Å) near the acyl-binding pocket, weak interactions
378 such as Van Der Waals' force with surrounding amino acid residues are also presented in the interaction.
379 The results suggest that CGA was located close to Ser153 and His264 (Fig. 4d1), which were reported to be
380 amino acid residues near an enzyme active site (Martinez-Gonzalez, et al., 2017), and explained the
381 inhibitory effect of CGA on lipase activities. The result is in good agreement with the competitive type of
382 inhibition obtained from former lipase-CGA inhibition assay.

383 For the LOX-CGA complex, CGA formed more hydrogen bonds (Fig. 4c2 and 4d2), including
384 conventional hydrogen bonds with glutamic (Glu) 357 (Bond length-2.87 Å, 2.03 Å) and Arg 403 (2.87 Å,
385 2.47 Å), carbon hydrogen bond with Glu 357 (3.04 Å), Arg 403 (2.35 Å) and phenylalanine (Phe) 175 (2.48

386 Å). Hydrophobic interactions also exist between the benzene ring of CGA and Arg 403 (4.47 Å), isoleucine
387 (Ile) 400 (5.35 Å) and Ile 173 (5.37 Å). Miscellaneous interactions like metal-acceptor (3.09 Å) formed
388 between Fe and CGA. It can be deduced that hydrogen bonds, hydrophobic interactions and the Van Der
389 Waals' force are the dominant interactive forces that promote the binding of LOX and CGA, which further
390 validate or reconfirm the results of fluorescence spectra analysis.

391

392 **4 Conclusions**

393 The experimental results showed the inhibitory effect of CGA on endogenous lipase and LOX in grass carp
394 muscle, and the inhibition types were competitive inhibition and mixed inhibition respectively. In the study,
395 the interaction mechanisms between CGA and enzymes were also investigated using multi-spectroscopy
396 methods combined with molecular docking studies. These results indicated the formation of enzyme-CGA
397 complexes and changes in enzymatic conformation during binding reactions. The intrinsic fluorescence
398 intensities in two types of enzymes were significantly quenched with CGA mainly through static quenching.
399 The hydrophilic microenvironment and polar environment surrounding aromatic amino acid residues in
400 enzymes resulting from CGA were reflected in the shifts in fluorescence spectra and UV-Vis spectra. The
401 changes in the CD spectra and FT-IR spectra showed that CGA had different effects on secondary structures
402 of lipase and LOX. The addition of CGA resulted in the aggregation of lipase as demonstrated from the
403 results of particle size analysis. Molecular docking analysis suggested that CGA may bind close to the active
404 site of lipase. Hydrogen bonds, hydrophobic interactions and the Van Der Waals' force were the main
405 interactions. The interactions between CGA and enzymes may provide a better understanding of the
406 inhibitory mechanism of CGA during the period of preservation, and in favor of its application in aquatic
407 products. This study could provide basic mechanisms of the inhibitory effects of polyphenols on lipid

408 oxidation during food preservation.

409

410 **Acknowledgement** This study was supported by the Nature Science Foundation of China (No. 31772047),
411 the Fundamental Research Funds for the Central universities (No. 2662019PY031 and 2662018JC056) and
412 the China Agriculture Research System (CARS-45-27).

413

414 **Authorship contribution statement**

415 **Qiongju Cao**: Methodology, Formal analysis, Writing - original draft. **Yuan Huang**: Methodology, Formal
416 analysis. **Quan-Fei Zhu**: Formal analysis; **Mingwei Song**: Conceptualization, Funding acquisition.
417 **Shanbai Xiong**: Academic instructor, Project administration. **Anne Manyande**: Writing - review & editing.
418 **Hongying Du**: Supervision, Conceptualization, Formal analysis, Funding acquisition, Writing - review &
419 editing.

420

421 **Conflict of interest**: The authors report no conflict of interest.

422

423 **Reference**

- 424 Andreou, A., Göbel, C., Hamberg, M., & Feussner, I. (2010). A bisallylic mini-lipoxygenase from cyanobacterium
425 *Cyanothece* sp. that has an iron as cofactor. *Journal of Biological Chemistry*, 285, 14178–14186.
- 426 Banerjee, S. (2006). Inhibition of mackerel (*Scomber scombrus*) muscle lipoxygenase by green tea polyphenols.
427 *Food Research International*, 39(4), 486-491.
- 428 Cao, Q., Du, H., Huang, Y., Hu, Y., You, J., Liu, R., Xiong, S., & Manyande, A. (2019). The inhibitory effect of
429 chlorogenic acid on lipid oxidation of grass carp (*Ctenopharyngodon idellus*) during chilled storage.
430 *Food and Bioprocess Technology*, 12(2019), 2050–2061.
- 431 Chauhan, P., Das, A. K., Nanda, P. K., Kumbhar, V., & Yadav, J. P. (2018). Effects of nigella sativa seed extract
432 on lipid and protein oxidation in raw ground pork during refrigerated storage. *Nutrition & Food Science*,
433 48(1), 2-15.
- 434 Cherif, S., & Gargouri, Y. (2009). Thermoactivity and effects of organic solvents on digestive lipase from
435 hepatopancreas of the green crab *Food Chemistry*, 116(1), 82-86.
- 436 Cysewski, P. (2008). A post-SCF complete basis set study on the recognition patterns of uracil and cytosine by
437 aromatic and π -aromatic stacking interactions with amino acid residues. *Physical Chemistry Chemical*
438 *Physics*, 10, 2636–2645.
- 439 Farhadian, S., Shareghi, B., Asgharzadeh, S., Rajabi, M., & Asadi, H. (2019). Structural characterization of α -
440 chymotrypsin after binding to curcumin: Spectroscopic and computational analysis of their binding

441 mechanism. *Journal of Molecular Liquids*, 289, 111111.

442 Gata, J. L., Pinto, M. C., & Macias, P. (1996). Lipoxygenase activity in pig muscle: purification and
443 partial characterization. *Journal of Agricultural and Food Chemistry*, 44(9), 2573-2577.

444 Ge, Y., Li, Y., Wu, T., Bai, Y., Yuan, C., Chen, S., Gakushic, I., & Hu, Y. (2020). The preservation effect of CGA-
445 Gel combined with partial freezing on sword prawn (*Parapenaeopsis hardwickii*). *Food Chemistry*, 313,
446 126078.

447 Gugliucci, A., Bastos, D. H. M., Schulze, J., & Souza, M. F. F. (2009). Caffeic and chlorogenic acids in *Ilex*
448 *paraguariensis* extracts are the main inhibitors of AGE generation by methylglyoxal in model proteins.
449 *Fitoterapia*, 80(6), 339-344.

450 He, W., Mu, H., Liu, Z., Lu, M., Hang, F., Chen, J., Zeng, M., Qin, F., & He, Z. (2018). Effect of preheat treatment
451 of milk proteins on their interactions with cyanidin-3-O-glucoside. *Food Research International*, 107,
452 394-405.

453 Huang, X., & Ahn, D. U. (2019). Lipid oxidation and its implications to meat quality and human health. *Food*
454 *Science and Biotechnology*, 28, 1275-1285.

455 Huo, Y., Du, H., Xue, B., Niu, M., & Zhao, S. (2016). Cadmium Removal from Rice by Separating and Washing
456 Protein Isolate. *J Food Sci*, 81(6), T1576-T1584.

457 Jiao, W., Shu, C., Li, X., Cao, J., Fan, X., & Jiang, W. (2019). Preparation of a chitosan-chlorogenic acid conjugate
458 and its application as edible coating in postharvest preservation of peach fruit. *Postharvest Biology and*
459 *Technology*, 154, 129-136.

460 Ju, J., Liao, L., Qiao, Y., Xiong, G., Li, D., & Wang, C. (2018). The effects of vacuum package combined with
461 tea polyphenols (v+tp) treatment on quality enhancement of weever (*micropterus salmoides*) stored at
462 0°C and 4°C. *LWT-Food Science and Technology*, 91, 484-490.

463 Karar, M. G. E., Matei, M.-F., Jaiswal, R., Illenberger, S., & Kuhnert, N. (2016). Neuraminidase inhibition of
464 dietary chlorogenic acids and derivatives-potential antivirals from dietary sources. *Food and Function*,
465 7(4), 2052-2059.

466 Kuepethkaew, S., Sangkharak, K., Benjakul, S., & Klomkiao, S. (2017). Use of TPP and ATPS for partitioning
467 and recovery of lipase from Pacific white shrimp (*Litopenaeus vannamei*) hepatopancreas. *Journal of*
468 *Food Science and Technology*, 54(12), 3880-3891.

469 Lakowicz, J. R. (2000). On Spectral Relaxation in Proteins. *Photochemistry and Photobiology*, 72(4), 421-437.

470 Lakowicz, J. R. (2006). Quenching of Fluorescence. *Principles of Fluorescence Spectroscopy*, 227-230.

471 Lowry, O. H., Rosebrough, N. J., Farr, A. L., & Randall, R. J. (1951). Protein Measurement with the Folin Phenol
472 Reagent. *Journal of Biological Chemistry*, 193(1), 265-275.

473 Martinez-Gonzalez, A. I., Alvarez-Parrilla, E., Díaz-Sánchez, Á. G., Rosa, L. A. d. I., Núñez-Gastélum, J. A.,
474 Vazquez-Flores, A. A., & Gonzalez-Aguilar, G. A. (2017). *In vitro* inhibition of pancreatic lipase by
475 polyphenols: a kinetic, fluorescence spectroscopy and molecular docking study. *Food Technology and*
476 *Biotechnology*, 55(4), 519-530.

477 Menezes, T. M., Almeida, S. M. V., Moura, R. O., Seabra, G., Lima, M. C. A., & Neves, J. L. (2019). Spiro-
478 acridine inhibiting tyrosinase enzyme Kinetic, protein-ligand interaction and molecular docking studies.
479 *International Journal of Biological Macromolecules*, 122(2019), 289–297.

480 Neguela, J. M., Poncet-Legrand, C., Sieczkowski, N., & Vernhet, A. (2016). Interactions of grape tannins and
481 wine polyphenols with a yeast protein extract, mannoproteins and β -glucan. *Food Chemistry*, 210(1),
482 671-682.

483 Nikpour, M., Mousavian, M., Davoodnejad, M., & Sadeghian, M. A. (2013). Synthesis of new series of
484 pyrimido[4,5-b][1,4] benzothiazines as 15-lipoxygenase inhibitors and study of their inhibitory

485 mechanism. *Medicinal Chemistry Research*, 22(10), 5036-5043.

486 Olthof, M. R., Hollman, P. C. H., & Katan, M. B. (2001). Chlorogenic Acid and Caffeic Acid Are Absorbed in
487 Humans. *The Journal of Nutrition*, 131(1), 66-71.

488 Peng, X., Zhang, G., Liao, Y., & Gong, D. (2016). Inhibitory kinetics and mechanism of kaempferol on α -
489 glucosidase. *Food Chemistry*, 190, 207-215.

490 Ross, P. D., & Subramanian, S. (1981). Thermodynamics of protein association reactions: forces contributing to
491 stability. *Biochemistry*, 20(11), 3096-3102.

492 Schreiber, R., Xie, H., & Schweiger, M. (2019). Of mice and men: The physiological role of adipose triglyceride
493 lipase (ATGL). *BBA-Molecular and Cell Biology of Lipids*, 1864(6), 880-899.

494 Shen, H., Zhao, M., & Sun, W. (2019). Effect of pH on the interaction of porcine myofibrillar proteins with
495 pyrazine compounds. *Food Chemistry*, 287(2019), 93-99.

496 Shi, J., Lei, Y., Shen, H., Hong, H., Yu, X., Zhu, B., & Luo, Y. (2019). Effect of glazing and rosemary (*Rosmarinus*
497 *officinalis*) extract on preservation of mud shrimp (*Solenocera melantho*) during frozen storage. *Food*
498 *Chemistry*, 272(30), 604-612.

499 Smichi, N., Gargouri, Y., Miled, N., & Fendri, A. (2013). A grey mullet enzyme displaying both lipase and
500 phospholipase activities Purification and characterization. *International Journal of Biological*
501 *Macromolecules*, 58, 87-94.

502 Sreeparna, B. (2006). Inhibition of mackerel (*Scomber scombrus*) muscle lipoxygenase by green tea polyphenols.
503 *Food Research International*, 39(2006), 486-491.

504 Su, J., Wang, H., Ma, C., Liu, C., Rahman, M. T., Gao, C., & Nie, R. (2016). Hypolipidemic mechanism of
505 gypenosides via inhibition of pancreatic lipase and reduction in cholesterol micellar solubility. *European*
506 *Food Research and Technology*, 242(3), 305-312.

507 Sun, Z., Zhang, X., Wu, H., Wang, H., Bian, H., Zhu, Y., Xu, W., Liu, F., Wang, D., & Fu, L. (2020). Antibacterial
508 activity and action mode of chlorogenic acid against *Salmonella* Enteritidis, a foodborne pathogen in
509 chilled fresh chicken. *World Journal of Microbiology and Biotechnology*, 36, 24.

510 Utrera, M., Morcuende, D., Ganhão, R., & Estévez, M. (2015). Role of Phenolics Extracting from *Rosa canina*
511 L. on Meat Protein Oxidation During Frozen Storage and Beef Patties Processing. *Food and Bioprocess*
512 *Technology*, 88(3), 854-864.

513 Xiong, G., Gao, X., Wang, P., Xu, X., & Zhou, G. (2016). Comparative study of extraction efficiency and
514 composition of protein recovered from chicken liver by acid-alkaline treatment. *Process Biochemistry*,
515 51, 1629-1635.

516 Xu, J., Hao, M., Sun, Q., & Tang, L. (2019). Comparative studies of interaction of β -lactoglobulin with three
517 polyphenols. *International Journal of Biological Macromolecules*, 136, 804-812.

518 Ying, M., Meti, M. D., Xu, H., Wang, Y., Lin, J., Wu, Z., Han, Q., Xu, X., He, Z., Hong, W., & Hu, Z. (2018).
519 Binding mechanism of lipase to Ligupurpuroside B extracted from Ku-Ding tea as studied by multi-
520 spectroscopic and molecular docking methods. *International Journal of Biological Macromolecules*,
521 120(2018), 1345-1352.

522 Yu, Q., Fan, L., & Duan, Z. (2019). Five individual polyphenols as tyrosinase inhibitors: Inhibitory activity,
523 synergistic effect, action mechanism, and molecular docking. *Food Chemistry*, 297(2019), 124910-
524 124920.

525 Zhu, J., Sun, X., Wang, S., Xu, Y., & Wang, D. (2017). Formation of nanocomplexes comprising whey proteins
526 and fucoxanthin: Characterization, spectroscopic analysis, and molecular docking. *Food Hydrocolloids*,
527 63, 391-403.

528 Zhu, M., Wang, L., Wang, Y., Zhou, J., Ding, J., Li, W., Xin, Y., Fan, S., Wang, Z., & Wang, Y. (2018).

529 Biointeractions of Herbicide Atrazine with Human Serum Albumin: UV-Vis, Fluorescence and Circular
530 Dichroism Approaches. *International Journal of Environmental Research and Public Health*, 15, 116.
531 Zhu, S., Yuan, Q., Yang, M., You, J., Yin, T., Hu, Y., & Xiong, S. (2019). A quantitative comparable study on
532 multi-hierarchy conformation of acid and pepsin-solubilized collagens from the skin of grass carp
533 (*Ctenopharyngodon idella*). *Materials Science & Engineering C*, 96(2019), 446-457.
534
535

536 **Table 1.** Quenching constants (K_{SV}), binding constants (K_a) and thermodynamic parameters of enzymes-
 537 CGA under different temperatures

	T (K)	K_{sv} (10^4 L/mol)	K_q (10^{12} L/mol·s)	R_a^2	K_a (10^5 L/mol)	n	R^2	ΔH (KJ/mol)	ΔS (J/mol·K)	ΔG (KJ/mol)
Lipase	298	2.11	2.11	0.990	0.33	1.05	0.998			-25.68
	304	1.67	1.67	0.997	0.16	0.99	0.996	-97.57	-241.23	-24.48
	310	1.55	1.55	0.995	0.07	0.92	0.995			-22.78
LOX	298	3.94	3.94	0.996	2.06	1.17	0.999			-30.56
	304	3.75	3.75	0.994	1.75	1.15	0.998	-63.76	-111.42	-30.00
	310	3.04	3.04	0.993	0.78	1.10	0.998			-29.22

538

539

540

541 **Table 2** Conformation changes in secondary structures of enzymes under difference treatments of CGA.

	Concentration of CGA (10^{-6} mol·L ⁻¹)	Secondary structure (%)			
		α -Helix	β -Sheet	β -Turn	Random coil
lipase	0	43.17	25.17	5.93	25.67
	20	41.05	27.40	6.50	25.00
	40	38.53	26.15	8.73	26.53
LOX	0	43.70	20.00	12.00	24.30
	20	44.03	23.73	9.03	23.17
	40	46.40	23.97	7.80	23.30

542

543

544

545 **Figures/Tables Legends**

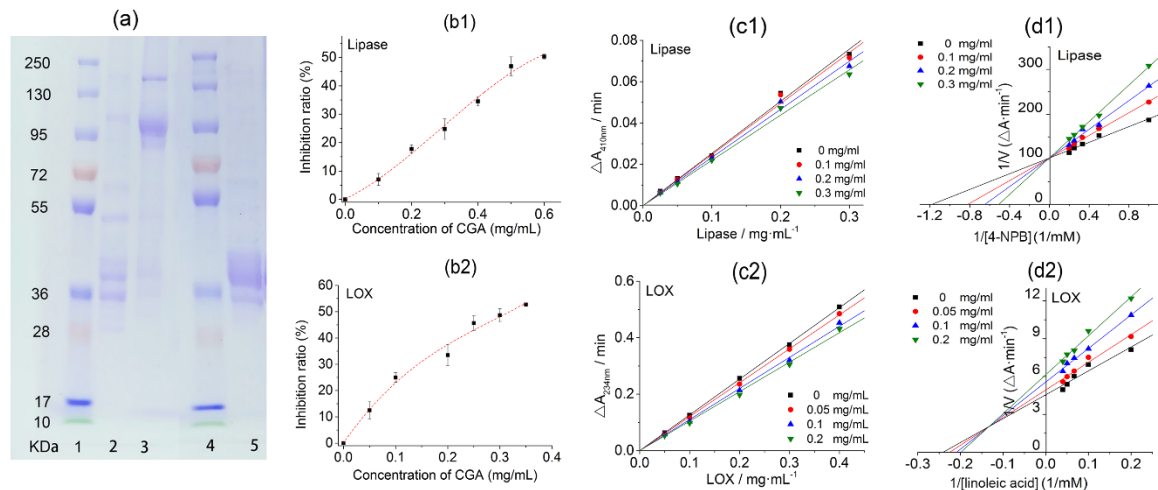
546 **Fig. 1** Results of purity of enzymes (SDS-PAGE) and inhibitory activities of lipase and LOX. *Note: a) 1*
547 *and 4-Markers; 2-Crude enzyme sample; 3-LOX; 5-Lipase; b) Inhibitory ratios of lipase (b1: $c_{lipase}=0.1$*
548 *mg/mL; $c_{4-npb}=3.0$ mM) and LOX (b2: $c_{LOX}=0.1$ mg/mL; $c_{linoleic\ acid}=20.0$ mM); c) Inhibitory types of lipase*
549 *(c1: $c_{4-npb}=3.0$ mM; $c_{CGA}=0.0-0.3$ mg/mL) and LOX (c2: $c_{linoleic\ acid}=15.0$ mM; $c_{CGA}=0.0-0.2$ mg/mL).*
550 *d) Inhibitory kinetics of lipase (d1: $c_{lipase}=0.1$ mg/mL; $c_{4-npb}=1.0-5.0$ mM; $c_{CGA}=0.0-0.3$ mg/mL) and*
551 *LOX (d2: $c_{LOX}=0.1$ mg/mL; $c_{linoleic\ acid}=5.0-25.0$ mM; $c_{CGA}=0.0-0.2$ mg/mL)*

552 **Fig. 2.** Fluorescence spectra analysis of the interaction between CGA and lipase (a1-d1) or LOX (a2-d2).
553 *Note: Figure legends: $c_{CGA}=0.0, 5.0, 10.0, 15.0, 20.0, 25.0, 30.0, 35.0, 40.0 \times 10^{-6}$ mol/L; a) Fluorescence*
554 *spectra ($T=298K$); b) Stern-Volmer plots for fluorescence quenching; c and d) Synchronous fluorescence*
555 *spectrum of lipase and LOX, $c-\Delta\lambda=15$ nm, $d-\Delta\lambda=60$ nm.*

556 **Fig. 3.** UV-VIS/FT-IR spectra and particle size analysis of lipase (a1-d1) or LOX (a2-d2) after the interaction
557 of CGA. *Note: Figure legends: $c_{CGA} \times 10^{-6}$ mol/L; a) UV-VIS absorption; b) FT-IR spectra; c)*
558 *Distribution of average particle size; d) Intensity of particle size distribution.*

559 **Fig. 4.** Molecular docking analysis of the interaction of CGA and lipase (a1-d1) or LDX (a2-d2). *Note: a)*
560 *and b): Docking ligand in the binding site; c) Results of 3D molecular docking modeling; d) Results of*
561 *2D molecular docking modeling.*

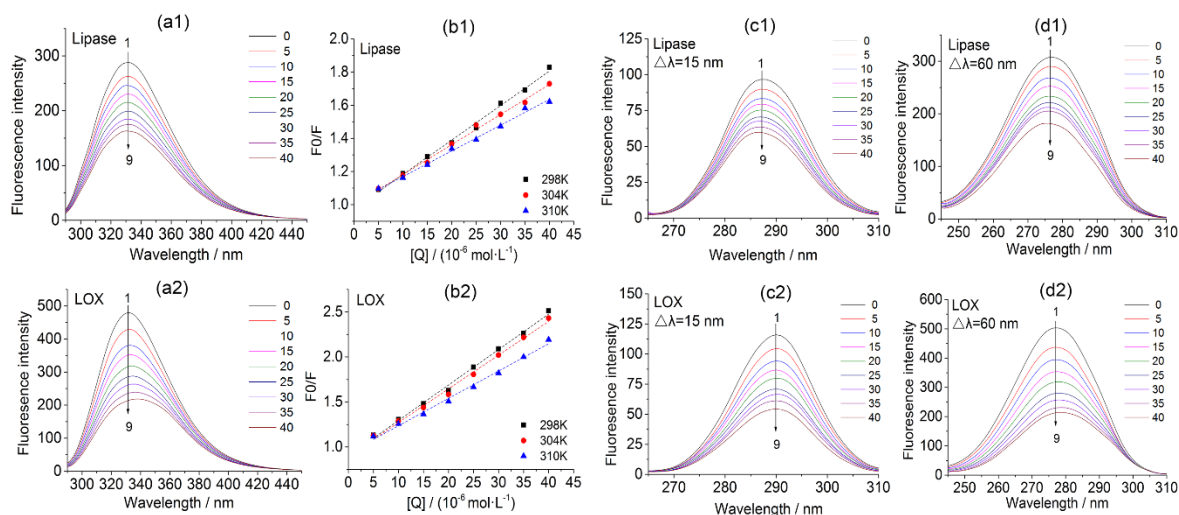
562



563

564 **Fig. 1** Results of purity of enzymes (SDS-PAGE) and inhibitory activities of lipase and LOX. *Note: a) 1*
 565 *and 4-Markers; 2-Crude enzyme sample; 3-LOX; 5-Lipase; b) Inhibitory ratios of lipase (b1: $c_{lipase}=0.1$*
 566 *mg/mL; $c_{4-npb}=3.0$ mM) and LOX (b2: $c_{LOX}=0.1$ mg/mL; $c_{linoleic\ acid}=20.0$ mM); c) Inhibitory types of lipase*
 567 *(c1: $c_{4-npb}=3.0$ mM; $c_{CGA}=0.0-0.3$ mg/mL) and LOX (c2: $c_{linoleic\ acid}=15.0$ mM; $c_{CGA}=0.0-0.2$ mg/mL).*
 568 *d) Inhibitory kinetics of lipase (d1: $c_{lipase}=0.1$ mg/mL; $c_{4-npb}=1.0-5.0$ mM; $c_{CGA}=0.0-0.3$ mg/mL) and*
 569 *LOX (d2: $c_{LOX}=0.1$ mg/mL; $c_{linoleic\ acid}=5.0-25.0$ mM; $c_{CGA}=0.0-0.2$ mg/mL)*

570



571

572

Fig. 2. Fluorescence spectra analysis of the interaction between CGA and lipase (a1-d1) or LOX (a2-d2).

573

Note: Figure legends: $c_{CGA} = 0.0, 5.0, 10.0, 15.0, 20.0, 25.0, 30.0, 35.0, 40.0 \times 10^{-6} \text{ mol/L}$; a) Fluorescence

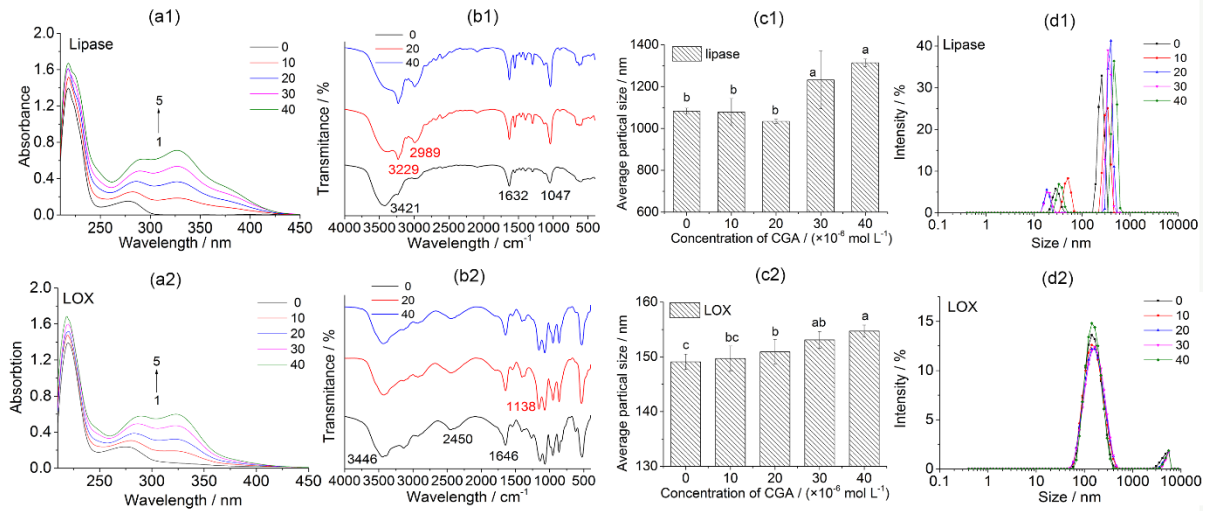
574

spectra ($T=298\text{K}$); b) Stern-Volmer plots for fluorescence quenching; c and d) Synchronous fluorescence

575

spectrum of lipase and LOX, c- $\Delta\lambda=15 \text{ nm}$, d- $\Delta\lambda=60 \text{ nm}$.

576



577

578

Fig. 3. UV-VIS/FT-IR spectra and particle size analysis of lipase (a1-d1) or LOX (a2-d2) after the

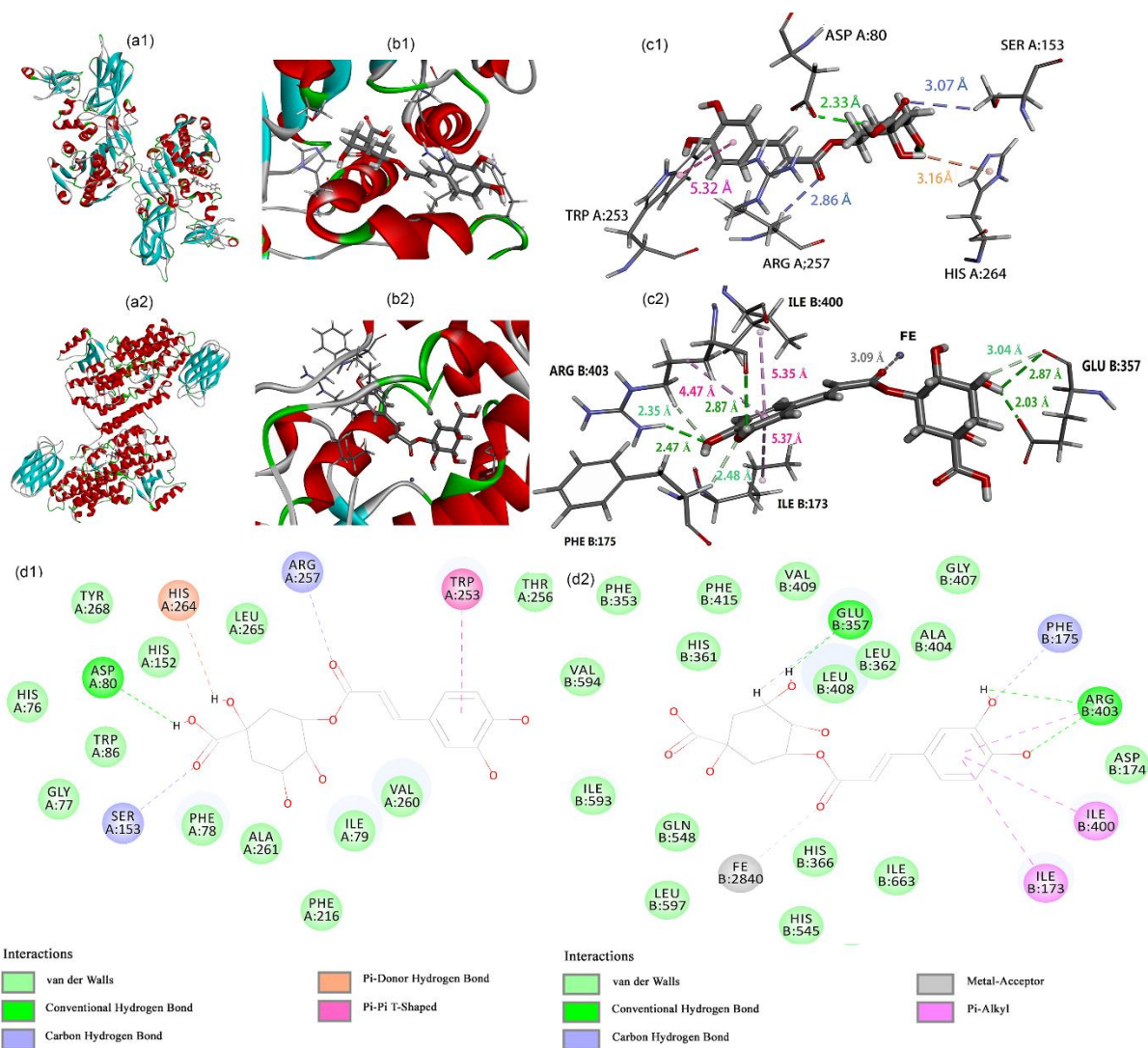
579

interaction of CGA. Note: Figure legends: $c_{CGA} = \times 10^{-6}$ mol/L; a) UV-VIS absorption; b) FT-IR spectra;

580

c) Distribution of average particle size; d) Intensity of particle size distribution.

581



582

583

Fig. 4. Molecular docking analysis of the interaction of CGA and ligase (a1-d1) or LDX (a2-d2). *Note:*

584

a) and b): Docking ligand in the binding site; c) Results of 3D molecular docking modeling; d) Results

585

of 2D molecular docking modeling.

586